

# Wild type and mutants of the HET-s(218–289) prion show different flexibility at fibrillar ends: A simulation study

Ran Friedman<sup>1,2,3\*</sup> and Amedeo Caflisch<sup>3\*</sup>

<sup>1</sup>Department of Chemistry and Biomedical Sciences, Linnæus University, 391 82, Kalmar, Sweden

<sup>2</sup>Linnæus University, Center for Biomaterials Chemistry, 391 82, Kalmar, Sweden

<sup>3</sup>Department of Biochemistry, University of Zürich, Winterthurerstrasse 190, CH-8057, Zürich, Switzerland

## ABSTRACT

The C-terminal segment (residues 218–289) of the HET-s protein of the filamentous fungus *Podospora anserina* is a prion-forming domain. The structural model of the HET-s(218–289) amyloid fibril based on solid-state nuclear magnetic resonance (NMR) restraints shows a  $\beta$  solenoid topology which is comprised of a  $\beta$ -sheet core and interconnecting loops. For the single-point mutants Phe286Ala and Trp287Ala, slower aggregation rates *in vitro* and loss of prionic infectivity have been reported recently. Here we have used molecular dynamics to compare the flexibility of the mutants and wild type. The simulations, initiated from a trimeric aggregate extracted from the NMR structural model, show structural stability on a 100-ns time scale for wild type and mutants. Analysis of the fluctuations along the simulations reveals that the mutants are less flexible than the wild type in the C-terminal segment at only one of the two external monomers. Analysis of interaction energy and buried accessible surface indicates that residue Phe286 in particular is stabilized in the Trp287Ala mutant. The simulation results provide an atomistic explanation of the suggestion (based on indirect experimental evidence) that flexibility at the protofibril end(s) is required for fibril elongation. Moreover, they provide further evidence that the growth of the HET-s amyloid fibril is directional.

Proteins 2013; 00:000–000.  
© 2013 Wiley Periodicals, Inc.

**Key words:** amyloid; aggregation; fibril growth; molecular dynamics.

## INTRODUCTION

Amyloid fibrils are (poly)peptide aggregates rich of  $\beta$ -sheet filamentous structures.<sup>1–5</sup> In many cases, these amyloid fibrils are a hallmark of a disease, such as Alzheimer's disease, Parkinson's disease and type II diabetes mellitus. A few amyloidogenic proteins, however, are associated with a biological function. One of these functional amyloids is the HET-s prion of the filamentous fungus *Podospora anserina*. Prion proteins exist mainly in two forms, monomeric (i.e., soluble) and fibrillar. The fibrillar form is infective, that is, can convert soluble prions into fibrils. Infection can take place by moving from cell to cell<sup>6</sup> and even between individuals. Creutzfeldt–Jakob disease, also known as transmissible spongiform encephalopathy, is an example of a rare human disease with a genetic or sporadic origin that can also be transmitted by consumption of bovine meat containing a prionic protein which infects native human proteins in the brain. The HET-s prion, however, carries out an important role in the life cycle of *P. anserina*. The colonies of this fungus

can grow side by side, that is, cells from two adjacent colonies may fuse together, mixing their cytoplasm and forming heterokaryons (cells with multiple nuclei of different origin). Vegetative fusion, as this process is called, can be advantageous for growth but carries out risk for transmission of infections such as viruses. To this end, *P. anserina* developed throughout its evolution an incompatibility mechanism involving the *het-s* genetic locus.<sup>7</sup> There are two *het-s* alleles, termed *het-s* and *het-S*.

Additional Supporting Information may be found in the online version of this article.

Grant sponsor: NCCR Neural Plasticity and Repair of the Swiss National Science Foundation; Grant sponsor: Research Program for Young Scientists of the University of Zürich; Olga Mayenfisch Foundation; Grant sponsor: Holcim Foundation; Grant sponsor: Linnæus University Center of Excellence for Biomaterials Chemistry.

\*Correspondence to: R. Friedman, Department of Chemistry and Biomedical Sciences, Linnæus University, 391 82 Kalmar, Sweden. E-mail: ran.friedman@lnu.se or A. Caflisch, Department of Biochemistry, University of Zürich, Winterthurerstrasse 190, CH-8057 Zürich, Switzerland. E-mail: caflisch@bioc.uzh.ch  
Received 20 March 2013; Revised 18 July 2013; Accepted 9 August 2013  
Published online 28 August 2013 in Wiley Online Library (wileyonlinelibrary.com).  
DOI: 10.1002/prot.24402

The first encodes the prionic protein HET-s that has two forms: soluble [HET-s\*] and prion-state [HET-s]. [HET-s] is infective and can convert the [HET-s\*] phenotype to [HET-s]. If a cell that carries the [HET-S] phenotype fuses with one that carries the prionic [HET-s] phenotype, the result is an incompatibility reaction and cell death due to membrane lesions,<sup>8</sup> but this is not the case with [HET-S] and [HET-s\*].

The structure of a fibril made by five units of the fibril-forming region of the HET-s protein has been elucidated by solid-state NMR in 2008.<sup>9</sup> Molecular dynamics (MD) simulations have provided evidence that this structure is preserved in solution on a 10-ns time scale.<sup>10</sup> Non-infectious fibrils were generated by aggregation at low-pH<sup>11</sup> and by mutations of the loop residues Phe286 or Trp287 to Ala.<sup>12</sup> It is not clear, however, why the mutations render the protein nonprionic, given the evidence that the final fibrillar structure is not affected by the mutations. Here, MD simulations of a trimeric unit of HET-s are analyzed to compare the flexibility of the wild-type (wt) and two single-point mutants. A trimer was preferred to a pentamer not only because it enables faster sampling but also to simplify the distinction between the external monomers and the monomer in the middle. The trimer is remarkably stable during the 100-ns time scale of the simulations, but the loop residues Phe286 and Trp287 are very mobile in one of the two external monomers. These residues are less flexible in the Phe286Ala and Trp287Ala mutants, so that the fibrillar end is more rigid and presumably less prone to sustain its growth.

## COMPUTATIONAL METHODS

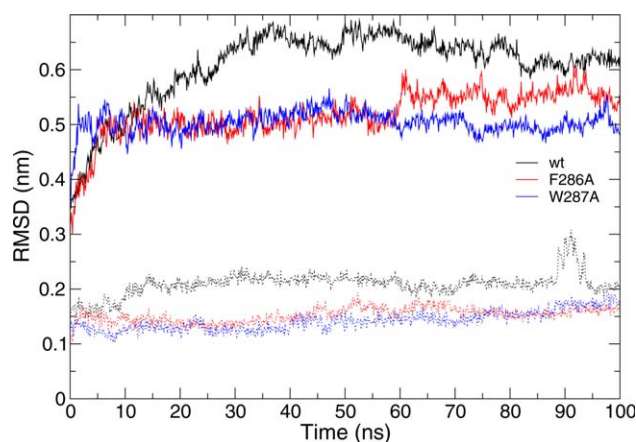
### Preparation of the molecular structure

The structure of truncated HET-s amyloid fibrils (pentamer of residues 217–289 and six His residues of the His tag)<sup>9</sup> was downloaded from the protein data bank (PDB). We simulated the structure with the His tag to allow comparison with the NMR structure, but it should be mentioned that the biological fibril includes a large, nonprionic domain and no residues beyond Asn289. The NMR structure file (PDB code: 2RNM) is a collection of 20 conformers. The stability of the individual configurations in solution was estimated by calculating the electrostatic contribution to the free energy assuming that the nonelectrostatic contribution (which is more difficult to calculate accurately) is much smaller. To this end, the APBS software<sup>13</sup> was used to calculate the free energy of solvation of each conformation by solving the non-linear Poisson-Boltzmann equation and adding the contribution from Coulombic interactions, using grid spacing of 0.045 nm and ionic strength of 0.1M. The third NMR conformer was used for the simulations as it had the most favorable electrostatic contribution to the free energy among the 20 NMR conformers. Note that in principle

another NMR conformer could have been chosen, as the equilibration part of the simulation is long enough and the core  $\beta$ -solenoid structure is similar among the 20 NMR conformers. To simulate a trimeric structure, chains B, C, and D (the middle chains) were extracted from the HET-s structure and the other chains were discarded. In addition, Phe286 and Trp287 were mutated individually to Ala *in silico* by removing the side chain atoms except for the C $\beta$  atom, mimicking the Phe286Ala and Trp287Ala single-point mutants, respectively. The protonation state of the titratable groups corresponds to pH = 7 conditions in all simulations. All side chains are neutral except for the arginine and lysine side chains, as well as the N-terminus, which are positively charged, and the glutamate and aspartate side chains, as well as the C-terminus, which are negatively charged.

### Molecular dynamics simulations

All simulations and preparations were performed by the Gromacs simulation package,<sup>14,15</sup> version 4.0.7. Energies and forces were calculated by use of the all-atom OPLS force field.<sup>16</sup> Each of the three structures was solvated in a truncated dodecahedron box so that the minimum distance between any protein atom and the edge of the box was 1.2 nm. The water molecules were modeled with the TIP4P model.<sup>17</sup> 43 Na<sup>+</sup> and 46 Cl<sup>-</sup> ions were added in order to neutralize the fibril charge and mimic an ionic strength of 0.1M. Ion force field parameters as developed by Åqvist<sup>18</sup> (Na<sup>+</sup>) and Chandrasekhar *et al.*<sup>19</sup> (Cl<sup>-</sup>) were used here. Before each MD simulation, internal constraints were relaxed by energy minimization, until the maximal force on individual atoms was smaller than 1 kJ mol<sup>-1</sup> nm<sup>-1</sup>. After the minimization, restrained MD runs were performed for 100 ps. During the restrained simulations, protein heavy atoms were fixed to their initial positions with a force constant of 1000 kJ mol<sup>-1</sup> nm<sup>-2</sup>. The restraints were released, and the system was equilibrated for 1 ns before data collection for analysis. During the MD runs, the LINCS algorithm<sup>20</sup> was used to constrain the lengths of bonds, while water molecules were kept rigid by use of the SETTLE algorithm.<sup>21</sup> Hydrogens were converted into virtual sites<sup>22</sup> and a 4 fs time step was used for integrating the equations of motion. The temperature was kept constant by use of the velocity-rescaling algorithm<sup>23</sup> ( $\tau_T = 0.1$  ps). The pressure was coupled to an external bath with Berendsen's coupling algorithm<sup>24</sup> ( $P_{ref} = 1$  bar,  $\tau_P = 1$  ps). Van der Waals forces were truncated at 1.0 nm with a plain cutoff. Long-range electrostatic forces were treated using the particle mesh Ewald method.<sup>25</sup> Each simulation was run for 100 ns. Analysis of the simulations was carried out by automatic tools available in Gromacs. Secondary structure analysis was performed with the DSSP algorithm.<sup>26</sup>

**Figure 1**

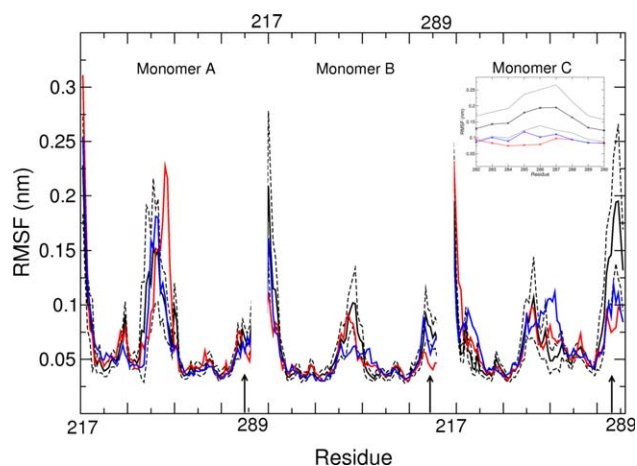
Root mean square deviations (RMSD) of all C $\alpha$  atoms (solid lines) and structural residues (dotted lines). The core of the trimeric structure is stable in all simulations. [Color figure can be viewed in the online issue, which is available at [wileyonlinelibrary.com](http://wileyonlinelibrary.com).]

## RESULTS AND DISCUSSION

### Structural stability of the HET-s trimer

The structural model of the HET-s(218–289) amyloid fibril was derived as a pentameric assembly from the solid-state NMR restraints.<sup>9</sup> Here we simulate a trimer, which enables us to infer on the directionality of the fibril by discriminating between its N-terminal, C-terminal and central unit. Note that the trimer has directionality, that is, one can distinguish the two external monomers, because of the topology of the  $\beta$  solenoid in which each HET-s(218–289) molecule forms two helical windings and individual monomers associate such that the fibrillar axis has the same directionality (N- to C-terminal) as the polypeptide chain itself. Examination of the structural residues which make up the core of the fibril and form  $\beta$ -sheets in the NMR structure (residues 227–233, 238–245, 263–269, and 274–281) reveals that they change very little during the simulations, for the wt protein and mutants alike (Fig. 1, dotted lines). The nonstructural residues, on the other hand, are very flexible and the C $\alpha$  root mean square deviation (RMSD) from the initial NMR conformer reaches values of 0.5–0.7 nm. Similar C $\alpha$  RMSD values are obtained when the 20 NMR conformers are compared to each other.

The secondary structure of the protein residues is maintained during the 100 ns simulations of the wt trimer (Supporting Information Fig. 1), which is another indication that the  $\beta$  solenoid topology is stable during the simulations. There are  $85 \pm 5$  residues with a defined secondary structure per  $\beta$  solenoid for the wt,  $82 \pm 6$  for the Phe286Ala mutant and  $87 \pm 6$  for the Trp287Ala mutant, as calculated over the second half of the simula-

**Figure 2**

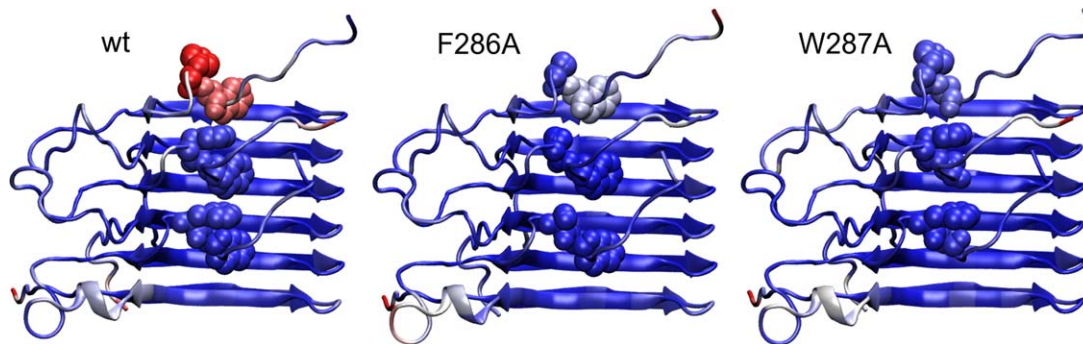
Root mean square fluctuations (RMSF) of the C $\alpha$  atoms calculated from the three MD ensembles: wt (black solid line, with dashed lines indicating average values  $\pm$  standard deviation), Phe286Ala (red) and Trp287Ala (blue). RMSF values are averages over 25 blocks of 2 ns, calculated between 50 and 100 ns of simulation time. The location of residue 286 (Phe in wt and Trp287Ala, Ala in Phe286Ala) is indicated by an arrow. Inset: RMSF of the C $\alpha$  atoms of wt (solid line, average; dashed line, standard deviation) and the mutants (red, Phe286Ala; blue, Trp287Ala). Only the region of the mutations for the C-terminal monomer is shown.

tions. Note that between 78 and 100 residues (on average  $88 \pm 5$ ) are in structural region the NMR ensemble. Monomer separation is not observed during the course of the 100-ns MD runs.

### The flexibility of monomers in the $\beta$ solenoid assembly

Neither experimental evidence nor our simulations indicate any significant difference in the fibrillar structure between the wt and mutant HET-s. Detailed structural information, however, is only available for the wt protein and we therefore compared the root mean square fluctuations (RMSF) along the MD simulations with those in the 20 NMR conformers (PDB code 2RNM). The MD trajectories and NMR ensemble show qualitatively similar profiles of RMSF along the sequence (Supporting Information Fig. 2). Quantitatively, the RMSF are larger in the NMR ensemble than along the MD runs but the values of the latter depend on the time interval used so that a direct comparison is not justified.

The fluctuations are largest at the termini of each monomer, and are similar between the monomers, with two exceptions (Fig. 2). Residues 244–254 are more mobile in the N-terminal monomer whereas residues 282–289 are more mobile in the C-terminal monomer. Interestingly, the flexibility of this region in the C-terminal monomer is drastically reduced upon mutation of Phe286 or Trp287 to Ala (Fig. 2, inset). In particular,

**Figure 3**

The structure of trimeric HET-s(218–289), colored according to the RMSF of the nonhydrogen atoms (average per residue; calculated along the 50–100 ns interval of each MD run). Blue stands for rigid residues, red for mobile. Residues 286 and 287 are shown in a sphere representation. Note that the 286/287 pair of the C-terminal monomer becomes less flexible upon mutation of Phe286 or Trp287 to Ala. [Color figure can be viewed in the online issue, which is available at [wileyonlinelibrary.com](http://wileyonlinelibrary.com).]

**Table I**

Mean Number of Contacts (Standard Deviation in Parentheses) Between the Side-Chain Atoms of Individual Side Chains and the Rest of the Protein in Simulations of wt and Mutant HET-s Trimers

	wt		Phe286Ala		Trp287Ala	
	Phe286	Trp287	Ala286	Trp287	Phe286	Ala287
Monomer A	41(6)	45(9)	13(2)	54(8)	43(9)	10(2)
Monomer B	37(7)	45(7)	15(3)	59(10)	48(9)	12(2)
Monomer C	26(5)	32(10)	10(1)	32(8)	39(8)	9(2)

A contact is defined as an atom within 0.4 nm of the side chain of Phe or Trp, or C $\beta$  of Ala.

residues Phe286 and Trp287 of the C-terminal monomer are highly flexible in the wt protein, but not in the mutants (Fig. 3).

Solid-state NMR measurements indicate that the side chain proton Trp287H $\epsilon$ 1 is water protected for weeks and that both Trp287 and Phe286 are relatively protected from polarization by the water, due to their location in a hydrophobic pocket.<sup>27</sup> The MD simulations reveal that the side chain of Phe286 of the C-terminal monomer is more buried in the Trp287Ala mutant than in wt (Supporting Information Fig. 3), while an opposite change is observed for Trp287 upon Phe286Ala mutation (Sup-

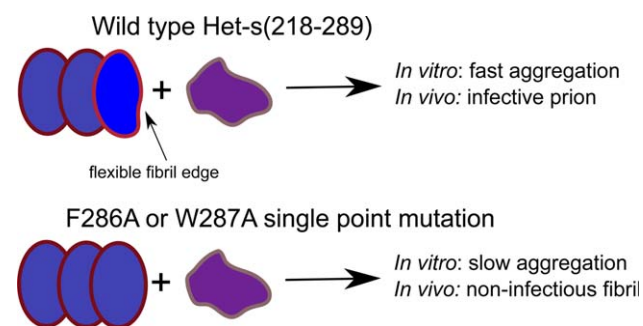
**Table II**

Interaction Energies Between the Side Chain of Phe286 or Trp287 of the C-terminal Monomer and the Other Residues of HET-s

	wt		Phe286Ala		Trp287Ala	
	Coulombic	vdW	Coulombic	vdW	Coulombic	vdW
Phe286-protein	-51(12)	-39(11)	-	-	-67(10)	-64(12)
Trp287-protein	-74(18)	-48(23)	-64(16)	-51(15)	-	-

The average values (and standard deviations in parentheses) are calculated along the second half of the trajectories and reported in kJ mol<sup>-1</sup>.

porting Information Fig. 4). Moreover, as reported by the time series of  $\chi^1$  and  $\chi^2$  dihedral angles (Supporting Information Fig. 5), the side chain flexibility of Phe286 is reduced upon Trp287Ala mutation. The reduced rotational disorder of Phe286 is due to additional contacts with neighboring residues upon mutation (Table I). Energy decomposition analysis for the interaction between Phe286 in the C-terminal monomer and the other residues reveals that the van der Waals contribution becomes more favorable upon Trp287Ala mutation by about 25 kJ mol<sup>-1</sup>, the Coulombic interactions by about 16 kJ mol<sup>-1</sup>, overall leading to increased stability of the Phe286 side chain (Table II).

**Figure 4**

Growth polarity and lower flexibility at the edge are a possible explanation of the reduction in aggregation rate upon mutation and lack of infectivity. HET-s(218–289) monomers (violet) are disordered and attach to one end of the fibril. In the simulations, the single-point mutants Phe286Ala and Trp287Ala show a less flexible C-terminal unit of the fibril than the wt, so that monomer attachment is slower. The simulation results provide an explanation for the slower aggregation rate of these mutants and their lack of infectivity. [Color figure can be viewed in the online issue, which is available at [wileyonlinelibrary.com](http://wileyonlinelibrary.com).]

## CONCLUSIONS

Explicit solvent molecular dynamics simulations of a trimeric aggregate of the fibril-forming domain of the HET-s protein (residues 218–289) were carried out to compare the wt with two single-point mutants (Phe286Ala and Trp287Ala) that are not infective *in vivo*. The flexibility of residues 282–289 in the C-terminal unit of trimeric wt HET-s(218–289) along the simulations suggests that fibril growth occurs primarily at one of the two ends of the  $\beta$  solenoid structure. This suggestion is based on the assumption that elongation requires a flexible fibrillar edge for allowing the binding of additional monomers, whose structure should be adapted. A mobile region is also observed at the N-terminal monomer. However, while the plasticity of the N-terminal monomer is similar between the wt and the mutants, the single-point mutation Phe286Ala or Trp287Ala results in stabilization of the C-terminal monomer. Growth polarization has been suggested recently on the basis of Monte Carlo simulations with a simplified model,<sup>28</sup> but the granularity of the model used (C $\alpha$  atoms only) is not sufficient to capture the differences between wt and (single-point) mutants.

*In vitro*, the single-point mutants Phe286Ala and Trp287Ala show slower aggregation kinetics than wt,<sup>12</sup> supporting the hypothesis that the growth is directional (or directionally preferred). The single point mutants Phe286Ala and Trp287Ala show stable  $\beta$  solenoid structure along the simulations. The higher flexibility of the C-terminal monomer of the wt suggests that the flexibility of the C-terminal region of the fibril is important for fibrillar elongation (Fig. 4). Structural and physiological studies have shown that the C-terminal domain of HET-s (residues 218–289) can aggregate and form fibrils whereas infectivity is a property of residues in the N-terminal domain.<sup>29</sup> It has previously been suggested that the N-terminal domain of HET-S interacts with the C-terminal and renders it less flexible.<sup>29</sup> Likewise, we propose that the mutant fibrils are less flexible and hence less prionic.

Finally, recent evidence<sup>8</sup> relates interactions between amyloid HET-s fibrils and non-compatible HET-S monomers to the incompatibility reaction. Apparently, the amyloid fibril can also induce structural changes in the nonamyloid HET-S, exposing a region with high membrane affinity. The modified HET-S proteins insert into the membrane, gradually causing membrane damage and cell death. It remains to be seen where this interaction takes place and whether the noninfective mutants are toxic. If they are not, it is likely that the HET-S/HET-s incompatibility reaction involves the flexible C-terminal domain as well.

## ACKNOWLEDGMENT

The authors are thankful to Roland Riek and Alice Soragni for interesting discussions and the anonymous

referees for their valuable comments. The simulations were carried out on the Schrödinger cluster of the University of Zürich.

## REFERENCES

- Sunde M, Blake C. The structure of amyloid fibrils by electron microscopy and X-ray diffraction. *Adv Protein Chem* 1997;50:123–159.
- Petkova AT, Ishii Y, Balbach JJ, Antzutkin ON, Leapman RD, Delaglio F, Tycko R. A structural model for Alzheimer's beta-amyloid fibrils based on experimental constraints from solid state NMR. *Proc Natl Acad Sci USA* 2002;99:16742–16747.
- Lührs T, Ritter C, Adrian M, Riek-Loher D, Bohrmann B, Döbeli H, Schubert D, Riek R. 3D structure of Alzheimer's amyloid-beta(1–42) fibrils. *Proc Natl Acad Sci USA* 2005;102:17342–17347.
- Tuite MF, Melki R. Protein misfolding and aggregation in ageing and disease: molecular processes and therapeutic perspectives. *Prion* 2007;1:116–120.
- Fändrich M. On the structural definition of amyloid fibrils and other polypeptide aggregates. *Cell Mol Life Sci* 2007;64:2066–2078.
- Brundin P, Melki R, Kopito R. Prion-like transmission of protein aggregates in neurodegenerative diseases. *Nat Rev Mol Cell Biol* 2010;11:301–307.
- Coustou V, Deleu C, Saupe S, Begueret J. The protein product of the het-s heterokaryon incompatibility gene of the fungus *Podospira anserina* behaves as a prion analog. *Proc Natl Acad Sci USA* 1997;94:9773–9778.
- Seuring C, Greenwald J, Wasmer C, Wepf R, Saupe SJ, Meier BH, Riek R. The mechanism of toxicity in HET-S/HET-s prion incompatibility. *PLoS Biol* 2012;10:e1001451.
- Wasmer C, Lange A, Van Melckebeke H, Siemer AB, Riek R, Meier BH. Amyloid fibrils of the HET-s(218–289) prion form a beta solenoid with a triangular hydrophobic core. *Science* 2008;319:1523–1526.
- Lange A, Gattin Z, Van Melckebeke H, Wasmer C, Soragni A, van Gunsteren WF, Meier BH. A combined solid-state NMR and MD characterization of the stability and dynamics of the HET-s(218–289) prion in its amyloid conformation. *Chembiochem* 2009;10:1657–1665.
- Wasmer C, Soragni A, Sabaté R, Lange A, Riek R, Meier BH. Infectious and noninfectious amyloids of the HET-s(218–289) prion have different NMR spectra. *Angew Chem Int Ed Engl* 2008;47:5839–5841.
- Soragni A, Wasmer C, Saupe SJ, Meier BH, Riek R. Infectious and non-infectious amyloids of the HET-s(218–289) prion: insights into assembly kinetic and structure of non-transmissible conformers. *Structure of Amyloid Fibrils and Mechanism of their Formation*, Halle an der Saale, Germany, P III-25. 2009.
- Baker NA, Sept D, Joseph S, Holst MJ, McCammon JA. Electrostatics of nanosystems: application to microtubules and the ribosome. *Proc Natl Acad Sci USA* 2001;98:10037–10041.
- Berendsen HJC, van der Spoel D, Vandrunen R. Gromacs—a message-passing parallel molecular-dynamics implementation. *Comput Phys Commun* 1995;91:43–56.
- van der Spoel D, Lindahl E, Hess B, Groenhof G, Mark AE, Berendsen HJC. Gromacs: fast, flexible, and free. *J Comput Chem* 2005;26:1701–1718.
- Jorgensen WL, Maxwell DS, Tirado-Rives J. Development and testing of the OPLS all-atom force field on conformational energetics and properties of organic liquids. *J Am Chem Soc* 1996;118:11225–11236.
- Jorgensen WL, Chandrasekhar J, Madura JD, Impey RW, Klein ML. Comparison of simple potential functions for simulating liquid water. *J Chem Phys* 1983;79:926–935.

18. Åqvist J. Ion-water interaction potentials derived from free energy perturbation simulations. *J Chem Phys* 1990;94:8021–8024.
19. Chandrasekhar J, Spellmeyer DC, Jorgensen WL. Energy component analysis for the hydration of Li<sup>+</sup>, Na<sup>+</sup>, F<sup>-</sup>, and Cl<sup>-</sup>. *J Am Chem Soc* 1984;106:903–910.
20. Hess B, Bekker H, Berendsen HJC, Fraaije JGEM. LINCS: a linear constraint solver for molecular simulations. *J Comp Chem* 1997;18:1463–1472.
21. Miyamoto S, Kollman PA. SETTLE: an analytical version of the SHAKE and RATTLE algorithms for rigid water models. *J Comp Chem* 1992;13:952–962.
22. Feenstra KA, Hess B, Berendsen HJC. Improving efficiency of large time-scale molecular dynamics simulations of hydrogen-rich systems. *J Comput Chem* 1999;20:786–798.
23. Bussi G, Donadio D, Parrinello M. Canonical sampling through velocity rescaling. *J Chem Phys* 2007;126:014101.
24. Berendsen HJC, Postma JPM, DiNola A, Haak JR. Molecular dynamics with coupling to an external bath. *J Chem Phys* 1984;81:3684–3690.
25. Darden T, York D, Pedersen L. Particle mesh ewald: an N-log(N) method for ewald sums in large systems. *J Chem Phys* 1993;98:10089–10092.
26. Kabsch W, Sander C. Dictionary of protein secondary structure: pattern recognition of hydrogen-bonded and geometrical features. *Biopolymers* 1983;22:2577–2637.
27. Van Melckebeke H, Schanda P, Gath J, Wasmer C, Verel R, Lange A, Meier BH, Böckmann A. Probing water accessibility in HET-s(218–289) amyloid fibrils by solid-state NMR. *J Mol Biol* 2011;405:765–772.
28. Baiesi M, Seno F, Trovato A. Fibril elongation mechanisms of HET-s prion-forming domain: topological evidence for growth polarity. *Proteins* 2011;79:3067–3081.
29. Balguerie A, Dos Reis S, Ritter C, Chaignepain S, Coulary-Salin B, Forge V, Bathany K, Lascau I, Schmitter JM, Riek R, Saupé SJ. Domain organization and structure-function relationship of the het-s prion protein of *Podospora anserina*. *EMBO J* 2003;22:2071–2081. Available at: URL <http://www.hubmed.org/display.cgi?uids=12727874>.